ADVANCED FUNCTIONAL MATERIALS
www.afm-journal.de

Biospecific Self-Assembly of a Nanoparticle Coating for Targeted and Stimuli-Responsive Drug Delivery

Jinyang Li, Xue Qu, Gregory F. Payne, Cheng Zhang, Yuxin Zhang, Jianbo Li, Jie Ren, Hua Hong, and Changsheng Liu**

Biology provides a range of materials, mechanisms, and insights to meet the diverse requirements of nanomedicine. Here, a biologically based nanoparticle coating system that offers three characteristic features is reported. First, the coating can be self-assembled through a noncovalent biospecific interaction mechanism between a lectin protein (Concanavalin A) and the polysaccharide glycogen. This biospecific self-assembly enables the coating to be applied simply without the generation of covalent bonds. Second, glycoprotein-based biofunctionality can be incorporated into the coating through the same noncovalent biospecific interaction mechanism. Here, the glycoprotein transferrin is incorporated into the coating since this moiety is commonly used to target cancer cells through a receptor-mediated endocytosis mechanism. Third, the coating can be triggered to disassemble in response to a reduction in pH that is characteristic of endosomal uptake. In a proof-of-concept study, comparing coated and uncoated nanoparticles, model drug-loaded nanoparticles (doxorubicin-loaded mesoporous silica nanoparticles) are prepared and it is observed that the coated nanoparticle has enhanced cytotoxicity for cancer cell lines but attenuated cytotoxicity for noncancerous cell lines. These studies demonstrate that biology provides unique materials and mechanism appropriate to meet the needs for emerging applications in the medical and life sciences.

1. Introduction

Advances in the medical and life sciences suggest exciting opportunities to enhance and personalize therapies, yet realizing this promise will require materials that meet exacting requirements. A common goal is for a therapeutic that is capable of recognizing aberrant cells (e.g., a cancer cell), and then selectively damaging, destroying, or reprogramming these cell types. Efforts to realize this ideal often employ nanoparticles to contain a therapeutic "payload" (e.g., a high dose of an anticancer drug), a coating to target the payload to the diseased cells, and a mechanism to trigger release of the payload.[1–5] Despite significant progress, many challenges remain in creating the smart materials needed to realize ideal nanomedicines.

While nanomedicine applications impose demanding requirements, biology provides a rich source of materials, mechanisms, and insights on how to meet these challenges.[6–8] In fact, biology routinely uses nanoparticles for the targeted delivery of payloads. For instance, viral pathogens target susceptible host cells for the delivery of nucleic acid payloads. Also, nerve cells engage in chemical communication using vesicles to deliver neurotransmitter payloads across synaptic junctions. In both these biological examples, the "payload" is enclosed within a nanoparticle which has a coating (e.g., composed of proteins and/or lipids) that offer three characteristics: the coating self-assembles; the coating has molecular recognition capabilities (e.g., for targeting); and the coating is smart and can be triggered to dump its contents in response to appropriate cues. Importantly, cues that are appropriate in biology (e.g., chemical, ionic, pH, and redox) are often quite different from the cues traditionally employed in technological smart materials (e.g., thermal, optical, and electrical). Thus, adapting biological approaches to create smart coating systems may be an important means to realize the promise of nanomedicine.

Here, we report the biologically based nanoparticle coating system based on sugar–lectin biorecognition between glycogen (Gly) and the tetra-functional lectin Concanavalin A (Con A).[9–14] As illustrated in **Scheme 1**, we provide evidence that this coating system offers three advantageous characteristics. First, the coating system can be self-assembled onto a

J. Li, Dr. X. Qu, C. Zhang, Y. Zhang, H. Hong, Prof. C. Liu
The State Key Laboratory of Bioreactor Engineering
East China University of Science and Technology
Shanghai 200237, China
E-mail: quxue@ecust.edu.cn;
liucs@ecust.edu.cn

J. Li, Dr. X. Qu, C. Zhang, Y. Zhang, H. Hong, Prof. C. Liu
Key Laboratory for Ultrafine Materials of Ministry of Education
East China University of Science and Technology
Shanghai 200237, China

Prof. G. F. Payne
Institute for Biosystems and Biotechnology Research
and Fischell Department of Bioengineering
5115 Plant Sciences Building
College Park, MD 20742, USA

Dr. J. Li, Prof. J. Ren
Institute of Nano and Biopolymeric Materials
School of Materials Science and Engineering
Tongji University
4800, Caoan Road, Shanghai 201804, China

DOI: 10.1002/adfm.201403636

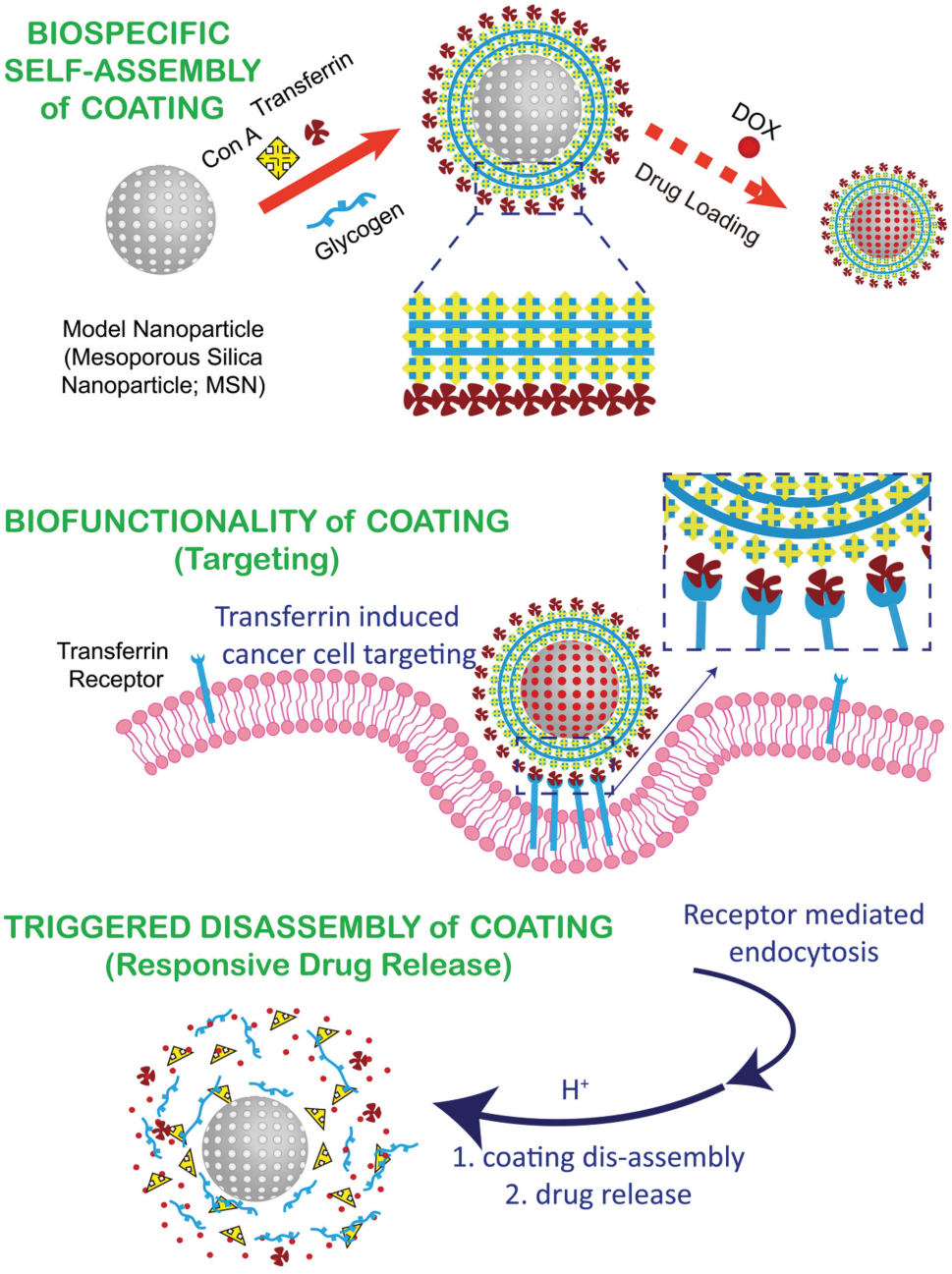

Scheme 1. Biology as a source of materials and mechanisms for functional coatings. Biospecific interactions are used to self-assemble a nanoparticle coating and incorporate biofunctionality, while the coating's responsive properties allow its disassembly to be triggered by biologically relevant cues.

nanoparticle through noncovalent and biospecific interaction mechanism. Second, a glycoprotein-based targeting moiety (i.e., transferrin (Tf)) can also be self-assembled into this Con A–glycogen coating system through the same noncovalent and biospecific protein–lectin binding mechanism.[15–17] Our targeting moiety, transferrin, is an iron-binding glycoprotein that can bind to cell surface transferrin receptors (TfR) and this binding induces a receptor-mediated endocytosis mechanism. Transferrin is commonly considered for nanoparticle targeting because (i) the transferrin receptor is upregulated by various cancer cells and thus targeting can be selective, and (ii) receptor-mediated endocytosis provides a mechanism for cell internalization.[3,18–22] Third, we show that the Con A–glycogen–transferrin coating system can be triggered to disassemble under the acidic conditions characteristic of endosomes (pH = 4.5–6.0).[23] To demonstrate the capabilities of our smart self-assembling coating, we performed proof-of-concept studies using mesoporous silica nanoparticles (MSN) and doxorubicin (DOX) as our model nanoparticle–drug system. We demonstrate that the Con A–glycogen–transferrin coating system enhances cytotoxicities for three cancerous cell lines but attenuates cytotoxicities for two noncancerous cell lines.

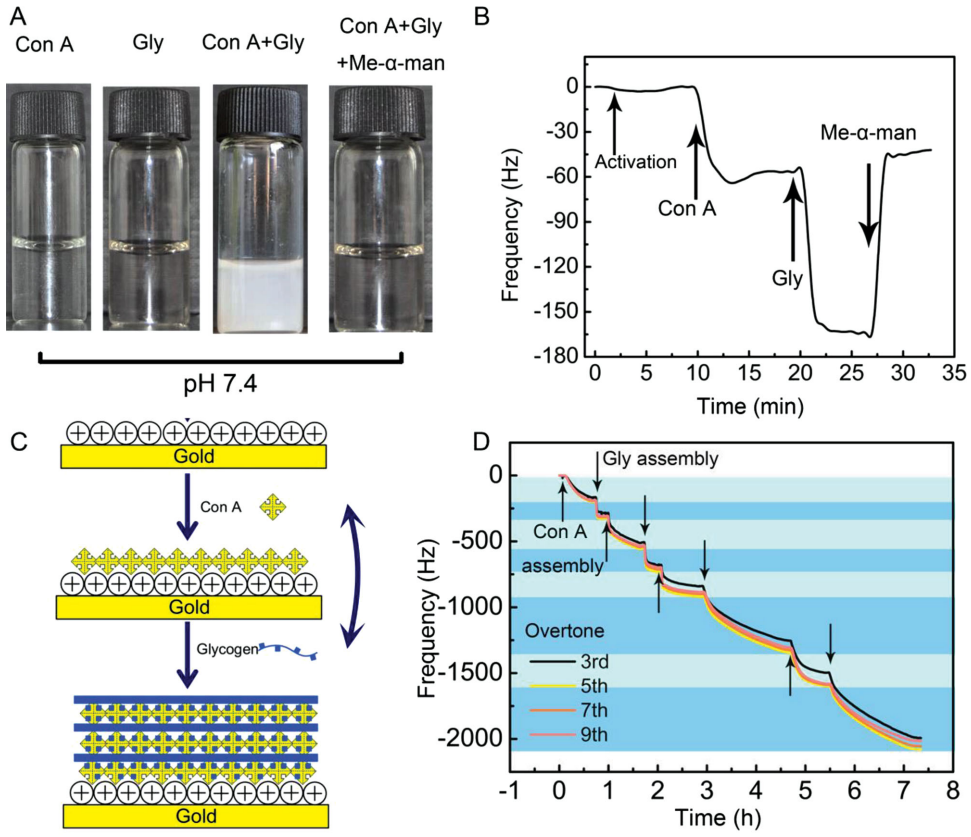

Figure 1. Biospecific self-assembly of Con A and glycogen (Gly). A) Photographs show that mixing Con A and glycogen at pH 7.4 yields precipitates and precipitation is inhibited by the competing monosaccharide Me-α-man. B) QCM-D evidence suggests that Me-α-man competes with and displaces glycogen for Con A binding. C) Schematic for Con A–glycogen multilayer self-assembly on quartz crystal. D) Experimental QCM-D results for self-assembly of this multilayer.

2. Results and Discussion

2.1. Biospecific Self-Assembly of Con A and Glycogen

Initially, we performed simple mixing studies to illustrate the biospecific binding between Con A and glycogen. The left two photographs in **Figure 1**A show that solutions of either Con A or Gly are transparent. When Con A and glycogen were mixed, a white precipitate was formed as shown in the third photograph of Figure 1A. This precipitate presumably results from a Con A-mediated crosslinking of glycogen to form an insoluble network. When methyl-α-D-mannopyranoside (Me-α-man) was mixed with Con A before adding glycogen, the rightmost photograph in Figure 1A shows no precipitate was formed. Me-α-man is known to bind strongly to Con A and presumably this monosaccharide blocks glycogen binding and prevents the formation of the insoluble Con A–glycogen network.[24] These results are consistent with biospecific protein–sugar interactions between Con A and glycogen as reported in refs. [10,25,26].

Independent evidence for biospecific interaction is provided by measurements from quartz crystal microbalance-dissipation (QCM-D). In this experiment, the gold surface of the quartz crystal was first activated using standard EDC/NHS chemistry.[27,28] Figure 1B shows that when a Con A solution (Tris–HCl with 1×10^{-3} M $MnCl_2$ and 1×10^{-3} M $CaCl_2$ buffered at pH 7.8) was contacted with this activated surface, the measured frequency decreases which is consistent with the successful coupling between the activated surface and the Con A. After rinsing, the Con A-modified surface was exposed to glycogen solution (Tris–HCl with 1×10^{-3} M $MnCl_2$ and 1×10^{-3} M $CaCl_2$ buffered at pH 7.8) and Figure 1B shows a rapid decrease in resonant frequency. This rapid decrease in frequency is consistent with the binding of glycogen to the Con A-modified surface. We next treated the surface with Me-α-man (5×10^{-3} M) and as seen in Figure 1B a rapid increase in frequency was observed. This frequency increase is consistent with a competitive displacement of the glycogen macromolecule ($M_w = 2.7 \times 10^5$–3.5×10^6 Da) by the Me-α-man monosaccharide ($M_w = 194$ Da). These results provide further evidence for biospecific sugar–lectin recognition between Con A and glycogen.

The Con A–glycogen coating was formed using layer-by-layer self-assembly as illustrated by the scheme in Figure 1C. Evidence for multilayer formation was provided using standard measurements from QCM-D. To initiate assembly, we first pretreated the gold surface of the quartz crystal with polyethyleneimine (PEI) to yield a positively charged surface that allows the first Con A layer to be assembled by electrostatic interactions. This crystal was then sequentially contacted with solutions containing Con A and glycogen. As shown in Figure 1D the frequency was observed to decrease monotonically with

each contacting step which is consistent with the sequential self-assembly of individual layer at each step. Interestingly, the observed frequency shifts show little dependence on the overtone number used which suggests that the assembled layers are relatively rigid.[29] These QCM-D results demonstrate self-assembly of Con A–glycogen multilayer and are consistent with results from other groups.[10,12,14]

2.2. Characterization

We next assembled a Con A–glycogen multilayer on MSN surface. MSN particles were prepared using well-known surfactant templating methods[30] and the TEM image in the upper left in **Figure 2**A shows the typical channel structure with an average particle diameter of 100–200 nm and pore diameter of 2–3 nm. The X-ray diffraction (XRD) analysis shows three low-angle reflections indexed as (100), (110), and (200) Bragg peaks, typical of a hexagonal mesoporous structure in MSN (Figure S1A, Supporting Information). To assemble the multilayer coating, we first applied a PEI pretreatment by incubating the MSN in a solution of PEI (4 mg mL^{-1}; 30 min). After rinsing, multilayer was assembled by sequentially contacting the MSN particles in solutions of Con A (2 mg mL^{-1}; 30 min) and glycogen (2 mg mL^{-1}; 30 min). TEM images in Figure 2A show MSN nanoparticles with different numbers of multilayer. These images show that the Con A–glycogen multilayer masks the original appearance of the MSN core and yielded a new cornea-like surface. These images also show that the Con A–glycogen coating with an outer Con A-layer has a granular structure with small particles of ≈5.1 nm in diameter, which corresponds to the size of the Con A protein ($4 \times 7.8 \times 8$ nm^3).

Chemical evidence for the self-assembled coating was obtained by comparing Fourier-transform infrared spectroscopy (FTIR) spectra for coated and uncoated MSN. Figure 2B shows that the spectra for a nanoparticle coated with four bilayers

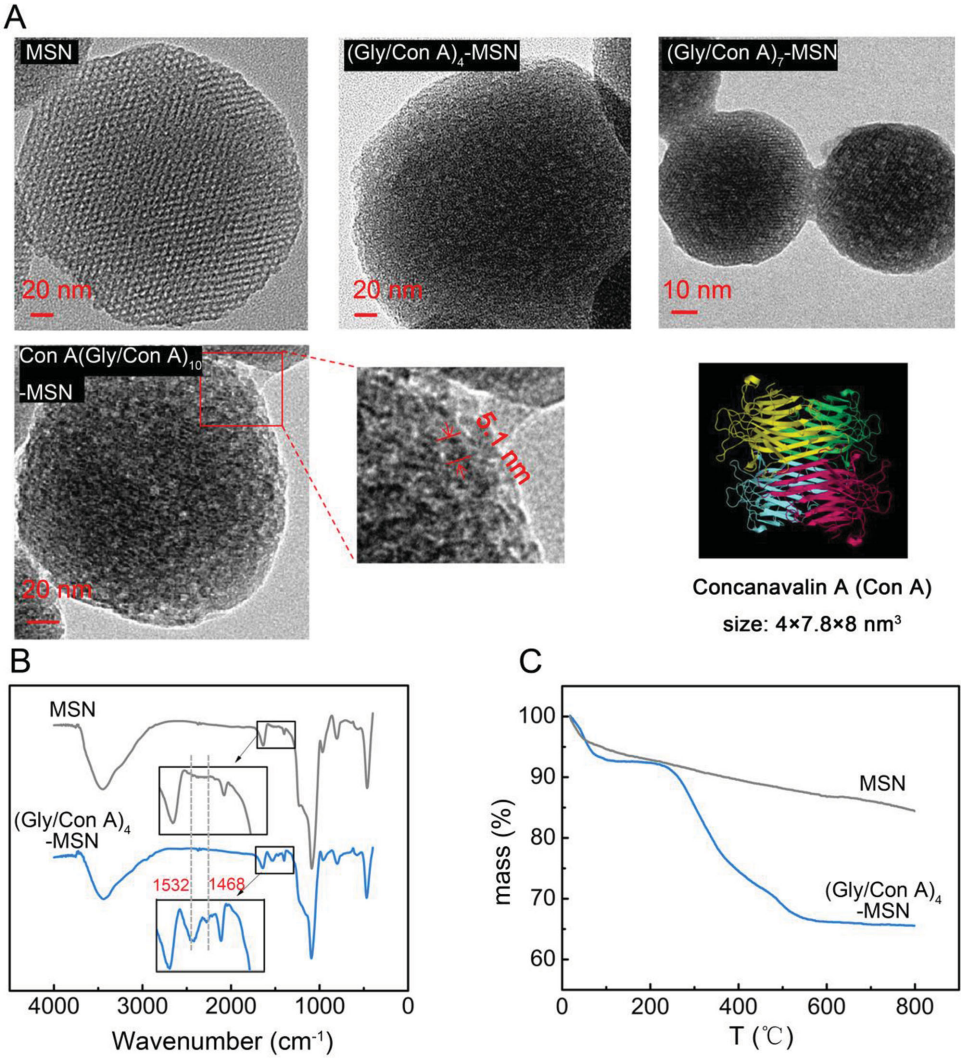

Figure 2. Characterization of coating. A) TEM images of nanoparticles (mesoporous silica nanoparticles (MSN)) with different numbers of multilayer (note granular structure possesses grains with a size comparable to that for Con A). B) FTIR spectra for MSN and $(Gly/Con\ A)_4$–MSN provide evidence for protein incorporation. C)TGA curves of MSNs and $(Gly/Con\ A)_4$–MSN indicate that the coating represents ≈20% of the coated nanoparticle's mass.

[(Gly/Con A)$_4$–MSN] shows absorption bands near 1532 and 1468 cm^{-1} which are assigned to the amide vibrations of the assembled Con A proteins. These results provide chemical evidence for protein incorporation into the self-assembled coating.

To estimate the extent of coating, we prepared nanoparticles with four bilayers [(Gly/Con A)$_4$–MSN] and then analyzed these nanoparticles by thermal gravimetric analysis (TGA). The top curve in Figure 2C shows results for the control uncoated MSN: a small loss of mass (11%) was observed as the temperature was increased to 800 °C. The value compares to the much larger loss of mass observed for coated MSN (34%). From these results we estimate that the ≈20% of the mass of the nanoparticle [(Gly/Con A)$_4$–MSN] is due to the Con A–glycogen coating.

2.3. Stimuli-Responsive Disassembly of Con A and Glycogen

Initial evidence that the association between Con A and glycogen is pH-dependent is provided by the photographs in **Figure 3**A. In this study, Con A and glycogen solutions were mixed at different pHs. Mixing at pH 7.4 resulted in turbid solutions indicating that precipitation had occurred. At pH 4, the mixed solution remained transparent indicating that Con A and glycogen were soluble. When the Con A and glycogen solutions were mixed at an intermediate pH of 5.0 an intermediate amount of turbidity was observed. These photographs are consistent with the explanation that Con A and glycogen interact to form an insoluble crosslinked network at pH 7.4, while such interactions are less favorable at lower pH. These observations are consistent with previous mechanistic studies that indicate: (i) sugar–Con A binding is reduced at low pH,[31] and (ii) Con A tetramers can dissociate into dimers as the pH is lowered.[32]

We use three independent methods to demonstrate pH-responsive disassembly of Con A–glycogen multilayer coating. First, we prepared a (Con A/Gly)$_4$ multilayer on a QCM crystal surface (e.g., as described in Figure 1C) and monitored changes in the frequency upon changing the solution pH. Figure 3B shows that lowering the buffer pH from 7.4 to 5.5 led to a dramatic increase in frequency. Further lowering the pH to 5 resulted in an additional dramatic increase in frequency. These increases in frequency are consistent with a loss of mass from the crystal surface (i.e., the multilayer is disassembling) when the pH is lowered.

In a second method to demonstrate pH-dependent disassembly, we coated MSN with a (Con A/Gly)$_4$ multilayer (e.g., as described in Figure 2A) using fluorescently labeled Con A. We then incubated these particles at different pHs and observed the appearance of Con A-fluorescence in the supernatant. Figure 3C shows little Con A-fluorescence appeared in the supernatant when the particles were incubated at pH 7.4, while rapid and significant Con A-fluorescence was observed when the particles were incubated at a pH of 5.0. These fluorescence measurements further indicate that the Con A–glycogen multilayer coating disassembles under acidic conditions.

The final method to demonstrate pH-dependent disassembly involved measurements of doxorubicin drug release from MSN-coated nanoparticles. In the experiment, the MSN particles were first coated with Con A–glycogen multilayer and then loaded with drug. Drug loading was achieved by incubating the (Con A–Gly)$_4$-coated MSN in solutions containing DOX(4 mg mL^{-1}, 5 mL pH 7.4) for 12 h. [Note: see Supporting Information for more details of the rationale and validation for loading drug after the coating has been assembled on the nanoparticle.] After drug loading, the particles were washed extensively in pH 7.4 buffer with little observed leakage of drug. In

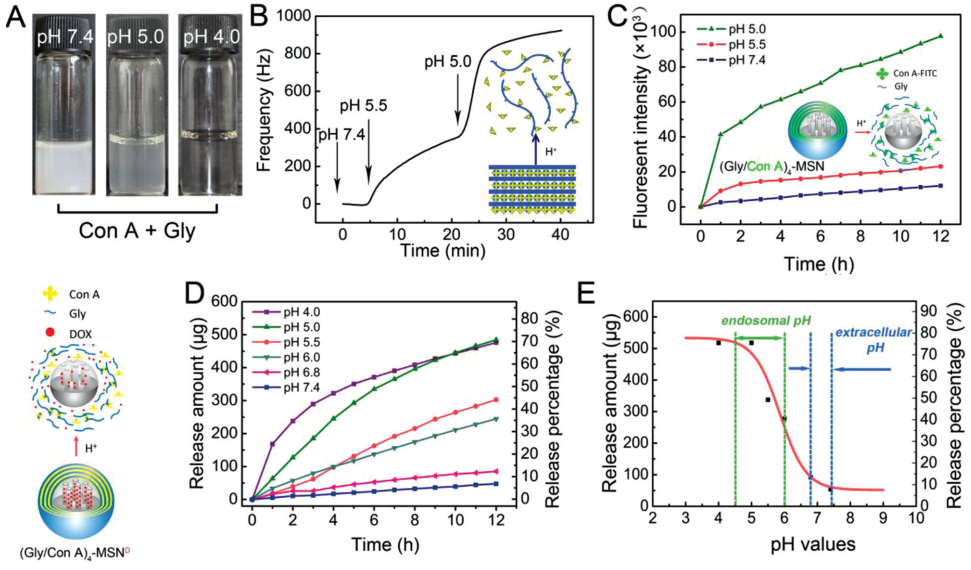

Figure 3. pH triggered disassembly of Con A–glycogen coating and release of the nanoparticle's cargo. A) Visual evidence indicates that Con A and glycogen form turbid solutions at pH 7.4 but form transparent solutions at pH 4.0, thus Con A–glycogen binding is pH-dependent. B) QCM-D evidence that disassembly of Con A–glycogen multilayer is triggered under acidic conditions. C) Fluorescence evidence (using FITC-labeled Con A) for disassembly of Con A–glycogen multilayer under acidic conditions. D) Fluorescence evidence (using DOX's intrinsic fluorescence) that drug release from Con A–glycogen MSNs [(Gly/Con A)$_4$–MSN^D] is triggered by low pHs. E) Cumulative drug release profiles as a function of pH from (Gly/Con A)$_4$–MSN after 12 h incubation.

contrast, uncoated MSN particles could be loaded with DOX, however much of this loaded drug was observed to leak from the uncoated-MSN particles upon subsequent buffer washing. We estimate the coated and drug loaded nanoparticles [(Con A–Gly)$_4$–MSN^D] contain about 7.0 wt% DOX (see Supporting Information). These observations suggest that the (Con A/Gly)$_4$ coating can limit egress of drug from the MSN nanopores under neutral conditions which suggests this coating can partially "gate" the MSN nanopores. Gating function is commonly reported for MSN-coatings.[33–35] However, the (Con A/Gly)$_4$ coating does not appear to offer complete gating function, otherwise it would be impossible to load the drug after the particle has been coated. These coated and drug-loaded nanoparticles were added to solutions buffered at varying pHs and drug release was measured spectrophotometrically. As illustrated in Figure 3D, DOX release was slow at pH 7.4, but was progressively more rapid in the acidic buffers. The pH-dependence of drug release from the (Gly/Con A)$_4$–MSN^D is summarized in Figure 3E.

In summary, the results in Figure 3 demonstrate that the Con A–glycogen-coated MSN particles display useful pH-dependent disassembly properties. At neutral pHs characteristic of extracellular conditions, the coating is stable and drug release is minimal. At the more acidic pH conditions that would occur during endosomal uptake, the coating becomes less stable and disassembles with a simultaneous release of drug. Interestingly, a comparison of Figure 3C and D indicates that at pH 5.5, Con A release is small while significant drug release is observed. This observation suggests the coating became more permeable at pH 5.5 but did not fully disassemble. Potentially, at pH 5.5, Con A had undergone its tetramer to dimer transition[36] without losing its glycogen-binding ability and thus some of the multilayer may have relaxed but otherwise remained intact.

We should note that several groups have reported that Con A–glycogen multilayer is glucose-responsive and can disassemble in the presence of glucose.[9,10,12] As shown in Figure S2B–D, Supporting Information), we observed that at pH 7.4 the multilayer is stable in the presence of physiologically relevant levels of glucose. At pH 5.5 however, glucose was observed to accelerate disassembly and drug release. Presumably, the comparatively weak binding of glucose to Con A[10] is insufficient to displace glycogen. The observation that the multilayer is stable in the presence of glucose under neutral conditions is important since many therapeutic applications would require the coating to remain intact in the presence of millimolar levels of glucose.[11]

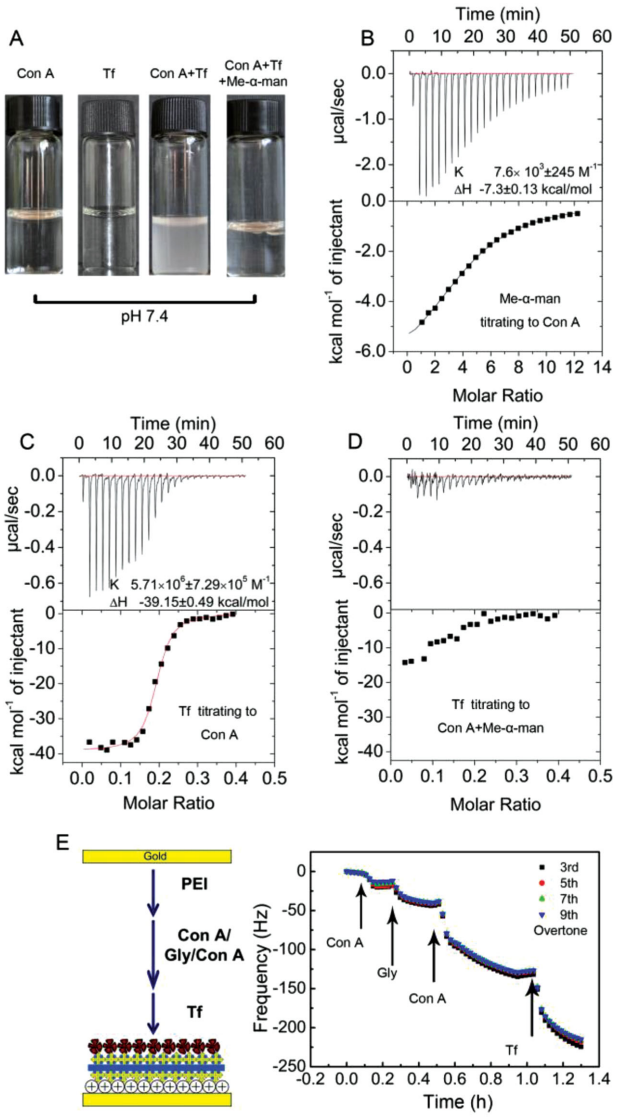

Figure 4. Biospecific self-assembly of transferrin (Tf) with Con A. A) Photographs show that mixing Con A and transferrin at pH 7.4 yields precipitates and precipitation is inhibited by the competing monosaccharide Me-α-man. B–D) Isothermal titration calorimetry (ITC) measurements show exotherms for the titration of Me-α-man or transferrin into Con A solutions, while titration of transferrin into Con A solutions containing Me-α-man show small exotherms (presumably transferrin competes with Me-α-man for Con A's sugar binding site). E) Schematic and experimental QCM-D results for self-assembly of transferrin into the Con A–glycogen coating.

2.4. Transferrin Assembly

Con A is known to bind a variety of sugars and glycoproteins[37–41] and thus provides a means to self-assemble various functionalities to the Con A–glycogen coating. In this study, we examined the incorporation of transferrin glycoproteins into the coating as a means to confer targeting and cellular uptake functionality.[18,42,43] Initial evidence that Con A recognizes and binds transferrin is provided by the photographs in **Figure 4**A. The left-most images show that Con A and Tf are each soluble at pH 7.4 while a mixture of these two proteins results in the formation of a precipitate. If transferrin is added into a solution containing both Con A and Me-α-man, limited precipitation is observed. The ability of Me-α-man to suppress Con A–transferrin precipitation provides initial evidence that this monosaccharide competes in a biospecific interaction between Con A and transferrin's sugar residues.[44,45]

More rigorous evidence for biospecific binding between Con A and transferrin was provided by isothermal titration calorimetry (ITC). An initial binding experiment was performed by adding Me-α-man to a solution of Con A at

pH 7.8. Figure 4B shows the typical exothermic heats for Me-α-man–Con A binding, while the calculated binding affinity (7.6×10^3 M^{-1}) and enthalpy (–7.3 kcal mol^{-1}) are consistent with previously reported values.[46,47] A second binding experiment was performed by adding transferrin to a Con A solution. The results in Figure 4C and the calculated thermodynamic properties demonstrate a considerably higher affinity (5.7×10^6 M^{-1}) and more favorable enthalpy (–39.1 kcal mol^{-1}) for transferrin–Con A binding. A final binding experiment was performed by adding transferrin to a solution containing both Con A and Me-α-man. Figure 4D shows small amounts of heat were evolved when transferrin was added which is consistent with the displacement of small amounts of Me-α-man from Con A binding sites (e.g., transferrin binding is more exothermic than Me-α-man).[48] The integrated heat evolution curve for the addition of transferrin became featureless in the presence of Me-α-man. The observation that Me-α-man disrupts transferrin binding provides further evidence that Con A binds transferrin through a biospecific interaction involving Con A's sugar binding site.

We next demonstrated the transferrin assembly into the Con A–glycogen coating by QCM-D method. As shown in Figure 4E, we first fabricated a Con A–glycogen coating with an outer Con A layer on the gold surface of the quartz crystal, and then exposed this surface to a solution containing transferrin (4 mg mL^{-1}). A decrease in the frequency was observed which indicates the successful incorporation of transferrin into the Con A–glycogen coating presumably through binding of transferrin's sugar chains to the outmost layer of Con A. The QCM-D result supports the hypothesis of self-assembly of functional glyco-species with Con A protein through the biospecific sugar–lectin interaction.

To prepare nanoparticles with transferrin incorporated into the coating, we incubated the Con A(Gly/Con A)$_4$–MSN with a transferrin solution. The amount of transferrin incorporated into the coating was estimated by UV–vis spectroscopy to be ≈80 μg (Tf) mg^{-1} (coated-MSN), which is comparable to values reported elsewhere for nanoparticles with covalently conjugated transferrin.[49]

2.5. Cell Studies

Initial biocompatibility studies were performed using a common human liver cancer cell line (HepG2). Specifically, we coated MSN with a Con A–glycogen multilayer (Con A outer layer), self-assembled transferrin to the coating, and then incubated HepG2 cells with these Tf/Con A/(Gly/Con A)4–MSN. Cells incubated with varying levels of coated MSN were observed to retain high viability after 24 and 48 h incubations (results shown in Figure S3, Supporting Information). This initial study indicates that the coating has no obvious cytotoxicities.

2.6. Transferrin Targeting Effect

The motivation of assembling glycoprotein transferrin onto our coating is due to its targeting biofunction to cancer cell lines. As mentioned, in various studies, transferrin-mediated selective endocytosis is employed for anticancer drug delivery,[3,22,50] cell imaging,[52] or understanding the cell-specific internalization of nanoparticles.[53] We initiated the cancer cell targeting studies of our Con A–glycogen–transferrin coating using the standard cell culture conditions consistent with the above cited papers' recommendation. Specifically, our cell culture media included serum which has been reported in some cases to disrupt transferrin-mediated nanoparticle targeting[49] and also glucose (25×10^{-3} M) which has been reported in some cases to competitively disassemble glycogen–Con A multilayers.[11,12]

As suggested in **Figure 5**A, binding of transferrin to its receptor initiates cellular uptake by a receptor-mediated endocytosis mechanism, and uptake tends to be selective because cancer cells overexpress the transferrin receptor.[54] Initial studies to demonstrate that the coating confers transferrin-mediated uptake were performed using confocal laser microscopy. In this experiment, MSN particles were fluorescently labeled with Texas Red and then coated with Con A–glycogen multilayer with or without transferrin. These particles were then added to proliferating cultures of the HepG2 cancer cell line which is known to overexpress the TfR.[19,55,56] After 3 h incubation, the cells were fixed, washed, and their nuclei stained.

The first column of images in Figure 5B shows results for cells exposed to the MSN particles that lacked any coating. Little red fluorescence is observed in these images indicating there was limited uptake of the uncoated MSN particles by the HepG2 cells. The second column of images in Figure 5B shows results for cells exposed to MSN particles coated with a Con A–glycogen multilayer (without transferrin). These images also show little red fluorescence indicating that the coating by itself does not substantially increase MSN particle uptake by these HepG2 cells. The third column in Figure 5B shows results for cells exposed to the MSN particles coated with a Con A–glycogen multilayer with transferrin. The images in this case show remarkable red fluorescence indicating considerable uptake of the MSN particles. Comparison of results from these three treatments indicates that incorporation of transferrin in the coating enhances cellular uptake of the MSN particles by these cancer cell lines.

To provide further evidence that the cellular uptake conferred by transferrin is receptor-mediated, we performed a competitive inhibition experiment. Specifically, we incubated HepG2 cells with both transferrin-functionalized MSN particles and free (i.e., soluble) transferrin. Comparison of the third and fourth columns in Figure 5B shows that the addition of free transferrin to the culture medium inhibits uptake of the transferrin-functionalized MSN particles. These results indicate that for the HepG2 cells, the incorporation of transferrin into the coating enhanced MSN particle uptake consistent with a receptor-mediated endocytosis mechanism.

To quantify transferrin's role in enhancing MSN particle uptake, we exposed HepG2 cells to particles with different coatings and then used flow cytometry to measure uptake of these Texas Red-labeled MSN particles (Figure 5C). The results from this study are reported as mean fluorescence intensity (MFI) in Figure 5D or percentage of cells that are positive for MSN particle uptake (Figure 5E). Figure 5C shows that cells treated with MSN particles with a Con A–glycogen multilayer coating showed a small increase in MFI value (1.46-fold) compared to

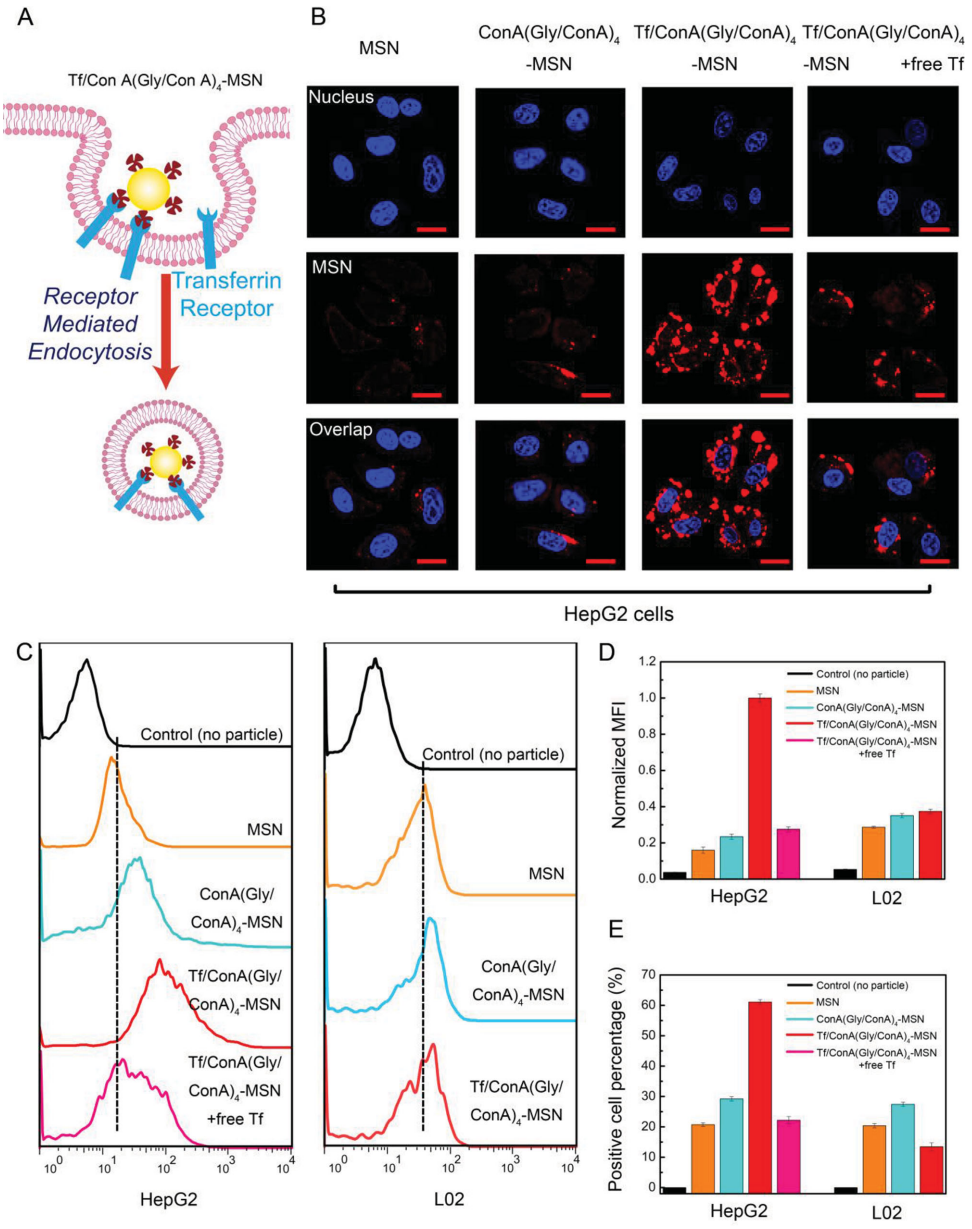

Figure 5. Transferrin confers targeting function for the selective endocytosis of nanoparticles to cancerous HepG2 cells. A) Schematic illustrates the targeting mechanism: binding between transferrin (Tf) and the transferrin receptor (TfR) engages receptor-mediated endocytosis while uptake is reduced if cells lack TfR or the solution contains free Tf. B) Confocal laser scanning microscopy images of nanoparticle-treated HepG2 cells show that the addition of Tf to the coating promotes cellular uptake and this uptake is inhibited by free Tf. Scale bar: 20 μm. C) fluorescence-activated cell sorting (FACS) provides quantitative evidence that transferrin in the coating targets the nanoparticle for uptake by the cancerous HepG2 cells, and noncancerous L02 cells can take up some uncoated nanoparticles but uptake is not substantially enhanced by transferrin in the coating. D,E) Summary of FACS results show that transferrin mediates nanoparticle targeting to HepG2 but not L02 cells based on either mean fluorescence intensity (MFI) or percent of cells that are positive for uptake [Data represent mean values ± SD ($n = 3$)].

cells treated with uncoated MSN particles. In contrast, cells treated with MSN particles with transferrin integrated into the coating showed a substantially larger MFI (6.25-fold increase). Finally, in a competitive inhibition study, we observed that cells treated with transferrin-coated MSN particles in the presence of soluble transferrin showed a 1.72-fold increase in MFI which is similar to the value observed for cells treated with transferrin-free MSN particles. These results are consistent with observations from confocal microscopy and further indicate that the addition of transferrin to the nanoparticle coating enhances cellular uptake through a biospecific mechanism.

To demonstrate that the cellular uptake conferred by transferrin is selective, we performed analogous experiments with a noncancerous human liver cell line, L02 cells. The flow cytometry analysis in Figure 5D,E indicates low and comparable mean fluorescence intensities were observed for cells treated with MSN particles irrelevant to whether the particles have coatings and whether the coatings include transferrin. This

result indicates that transferrin does not enhance MSN particle uptake for the L02 cells presumably because the L02 cells lack the transferrin receptor responsible for uptake. Comparison of the results between HepG2 and L02 cells indicates that the transferrin-mediated uptake of the MSN particles is selective for the HepG2 cancer cell line.

These results together indicate that multilayer coatings attached with transferrin layer can direct nanoparticles to selectively target cancer cells to a greater extent than for healthy cells. To our knowledge, this is the first demonstration of a biospecific self-assembling coating system for targeted nanoparticle delivery.

2.7. Intracellular Disassembly of Multilayer Coatings

We next tested whether cellular uptake of the nanoparticles was also associated with disassembly of the multilayer coating. As noted, uptake and processing through an endosomal pathway should expose the nanoparticles to the low pH conditions that trigger disassembly of the transferrin–Con A–glycogen multilayer coatings illustrated in **Figure 6**A. In this experiment, we prepared nanoparticles with dual fluorescence: MSN was fluorescently labeled with Texas Red and Con A in the coating was fluorescently labeled with FITC. These dual-labeled Tf/Con A(Gly/Con A)$_4$–MSN particles were then added to proliferating cultures of HepG2 and L02 cells. At varying times samples were fixed, washed, and the cell nuclei were stained, after which the samples were observed using confocal laser scanning microscopy. Figure 6B shows that the red fluorescence for the HepG2 cells appears to be particulate consistent with aggregates of MSN nanoparticles. In contrast, the green fluorescence of the HepG2 cells appears more diffuse within the cell which is consistent with disassembly of the FITC-labeled Con A coating. Over time, Figure 6B shows increasing intensities for both the particulate red fluorescence (MSN) and the diffuse green fluorescence (Con A). Figure 6C shows results with the noncancerous L02 cell lines. Again, the red fluorescence (MSN) was observed to be particulate in nature while the green fluorescence (Con A) was observed to be diffuse within the cells which is consistent with results for the HepG2. In contrast, the fluorescence intensities of the L02 cells were considerably lower consistent with the targeting capabilities of transferrin. The results in Figure 6 indicate that upon cellular uptake, the Con A–glycogen–transferrin coating disassembles presumably due to the low endosomal pH.

2.8. Intracellular Drug Release

We performed an analogous experiment to ensure that disassembly of the Con A–glycogen–transferrin coating upon cellular uptake is also associated with release of a drug loaded into the MSN nanoparticles (MSN^D) as illustrated in **Figure 7**A. As in the above experiment we fluorescently labeled the MSN particles with Texas Red, however in this experiment, the Con A was unlabeled. Drug release could be readily observed because of the intrinsic fluorescence of our model drug DOX. Analogous to the previous experiment, DOX-loaded Tf/Con A(Gly/Con A)$_4$–MSN particles were added to proliferating HepG2 and L02 cultures at a DOX dose of 0.5 μg mL^{-1} and samples were analyzed at varying times using confocal laser scanning microscopy.

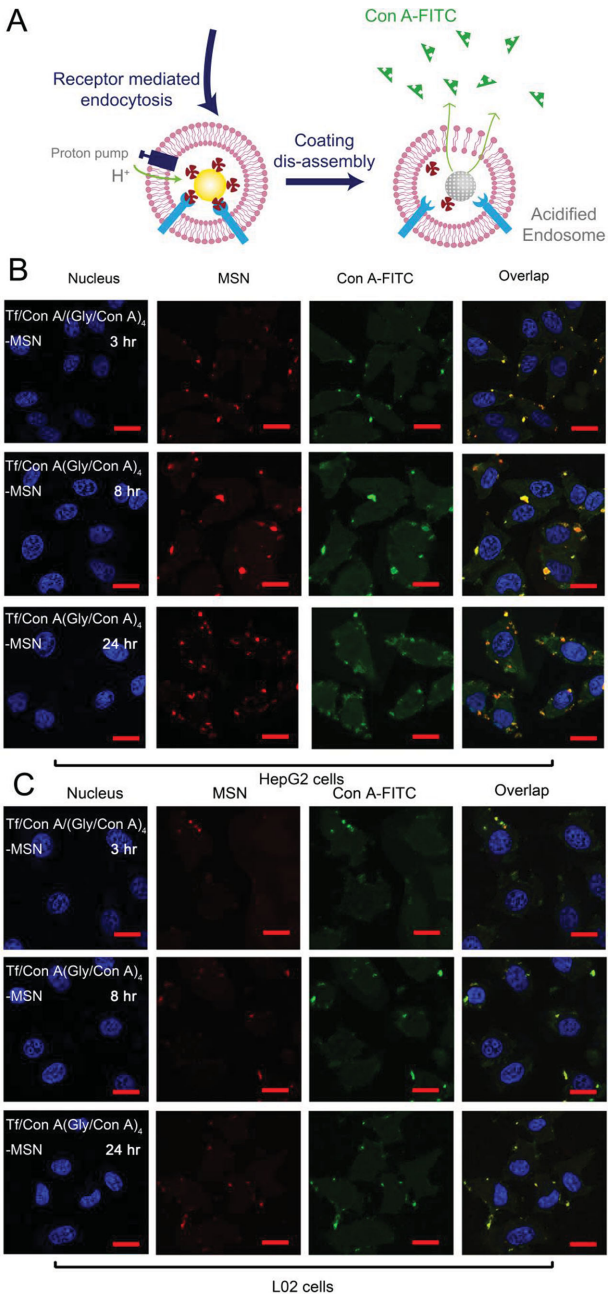

Figure 6. Intracellular disassembly of Con A–glycogen–transferrin coating. A) Schematic illustrates that disassembly of the coating is triggered by the acidic endosome. B) Confocal images of cancerous HepG2 cells treated with nanoparticles [Tf/Con A(Gly/Con A)$_4$–MSN] show that the red fluorescence (Texas Red-MSN) is particulate while the green fluorescence (FITC–Con A) is diffuse consistent with disassembly of the coating. C) Confocal images for analogous nanoparticle-treated L02 cells show analogous results although considerably lower overall fluorescence intensities (i.e., fewer nanoparticles entered these noncancerous L02 cells). Scale bar: 20 μm.

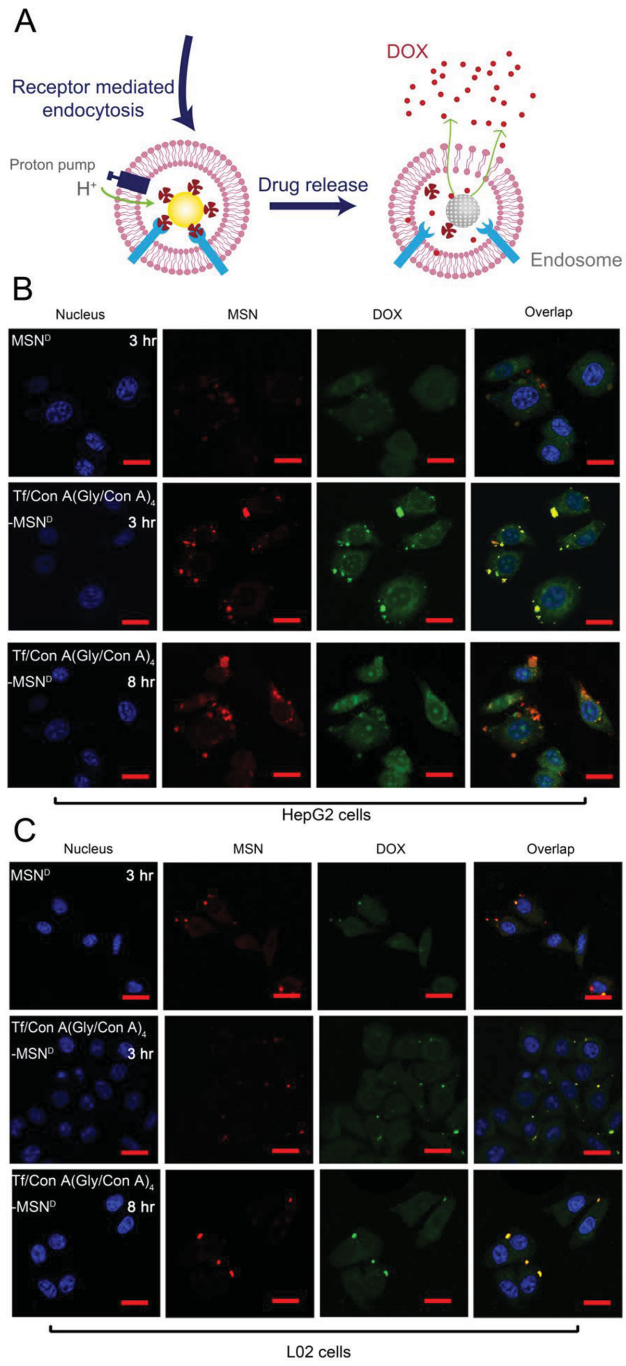

Figure 7. Targeted drug delivery to cancerous cells by Con A–glycogen–transferrin coating. A) Schematic illustrates that targeting and intracellular disassembly allow the nanoparticle's contents to be selectively delivered to the cancer cells. B) Confocal images of cancerous HepG2 cells treated with drug-loaded nanoparticles [Tf/Con A(Gly/Con A)$_4$–MSN^D; 0.5 μg mL^{-1} DOX] show that the red fluorescence (Texas Red-MSN) is particulate while the green fluorescence (DOX) is diffuse consistent with disassembly of the coating and release of the drug. C) Confocal images for analogous nanoparticle-treated L02 cells show analogous results although considerably lower overall fluorescence intensities (i.e., fewer nanoparticles entered these noncancerous L02 cells). Scale bar: 20 μm.

The first observation in Figure 7B concerns the effect of the coating on drug uptake by the HepG2 cells. When these cells were exposed for 3 h to control DOX-loaded MSN particles without a coating, MSN^D, only minimal amounts of red fluorescence (MSN) was observed in the cells. These control cells were also observed to have weak green fluorescence (from DOX) distributed within the cells. In contrast, Figure 7B shows that HepG2 cells incubated for 3 h with DOX-loaded MSN particles with the Con A–glycogen–transferrin coating, were observed to have significant particulate red fluorescence (MSN) and also significant diffuse green fluorescence (DOX) within the cells. This observation is consistent with the flow cytometry results and further demonstrates the importance of the Con A–glycogen–transferrin coating for nanoparticle targeting to the HepG2 cancer cell line.

The second observation in Figure 7B concerns the accumulation of drug over time for the HepG2 cells. Images for HepG2 cells incubated with Tf/Con A(Gly/Con A)$_4$–MSN^D for 8 h show more red fluorescence (MSN) and green fluorescence (DOX) compared to cells incubated with the same particles for 3 h. Again, the particulate nature of the red fluorescence is consistent with aggregates of MSN nanoparticles while the diffuse nature of the green fluorescence is consistent with the release of the DOX drug within the cell. Interestingly, the merged images in Figure 7B show yellow fluorescent particles for the 3 h samples but the 8 h samples show orange-colored particles. Potentially, the yellow particles observed after 3 h are due to the overlapping fluorescence of DOX and the labeled MSN particle, while the orange color observed after 8 h may indicate that the MSN particles contain less DOX at this later time. This explanation would indicate that disassembly of the coating observed upon cellular uptake (i.e., Figure 6) is associated with release of the DOX drug.

A final observation is shown in Figure 7C and concerns the noncancerous L02 cell line. Figure 7C shows that there was relatively little DOX uptake by the L02 cells treated for 3 h with MSN particles with or without the Con A–glycogen–transferrin coating. Presumably, the lack of targeting to the L02 cells reflects a low level of TfR for these cells. Even after 8 h, the uptake of MSN particles and intracellular accumulation of drug appears to be small. These observations further support the role of the coating's ability to selectively target cells that overexpress a specific biomarker while limiting uptake by other cells.

2.9. Effect of the Coating on Drug Cytotoxicity

The final step in this study was to evaluate the effect of the MSN coating on drug-mediated cytotoxicity using DOX as the model anticancer drug. Three cancer cell lines of HepG2, MDA-MB-231 (human breast adenocarcinoma cell line), and MGC-803 (human gastric cancer cell line) were, respectively, added with drug-loaded particles at a fixed drug dose of 2 μg mL^{-1}. After incubation for 48 h, the viability of the cells was measured by MTT assay. The first set of data in **Figure 8**A shows results from these HepG2 cells. The cells exposed to uncoated MSN^D were observed to have lower cell viabilities compared to the untreated control—presumably drug had leaked from these uncoated particles. The viability of cells exposed to

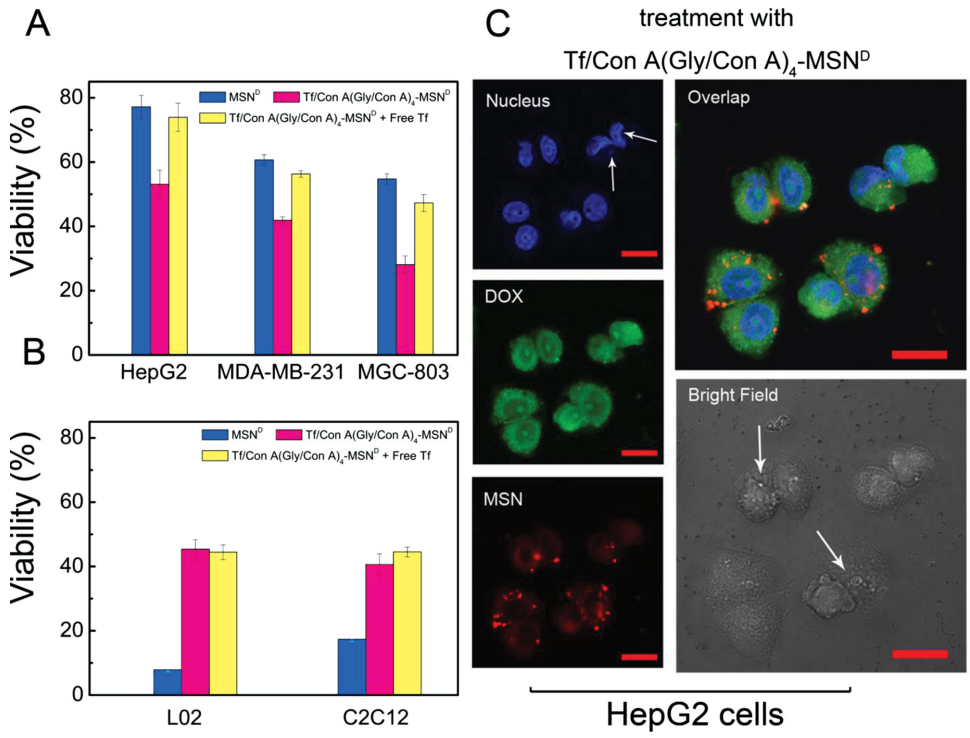

Figure 8. Transferrin in the coating enhances the cytotoxicity of drug-loaded nanoparticles for cancerous cell lines but attenuates the cytotoxicity for noncancerous cell lines. A) Viability of three different cancer cell lines challenged with drug-loaded nanoparticles that were uncoated (MSN^D), coated ($Tf/Con\ A(Gly/Con\ A)_4$–MSN^D), or coated but incubated with free Tf (incubations performed for 48 h with DOX dose of 2 μg mL^{-1}). B) Analogous results with two noncancerous cell lines. Note that all the values are normalized against the control of cells without drug treatment. Viability was measured by MTT method and data represent mean values ± SD ($n = 6$). C) Fluorescence and bright field images for HepG2 cells treated with nanoparticles [$Tf/Con\ A(Gly/Con\ A)_4$–MSN^D] are consistent with a cell apoptotic death mechanism (incubations performed for 24 h with DOX dose 0.5 μg mL^{-1}).

$Tf/Con\ A(Gly/Con\ A)_4$–MSN^D was observed to be further reduced. The addition of free transferrin to the incubation mixture prevented the transferrin-enhanced HepG2 killing. These results are consistent with the flow cytometry studies in Figure 5 and intracellular drug release results in Figure 7B and demonstrate that the incorporation of transferrin into the coating enhances the drug transfer into cells and thus results in an improved cell killing effect.

The second and third sets of data in Figure 8A are from MDA-MB-231 and MGC-803 cancer cells. The same trends were shown as observed for the HepG2 cancer cell lines. Specifically, the incorporation of transferrin into the coating enhances cytotoxity of MSN^D for these cancer cell lines. (Note: since our focus is the coating, we made no effort to optimize DOX levels which can have complex and varied effects on different cell lines.[57,58] Specifically, the incorporation of transferrin into the coating enhances cytotoxity of MSN^D for these cancer cell lines.

We further tested the cytotoxity of uncoated MSN^D and $Tf/Con\ A(Gly/Con\ A)_4$–MSN^D for two noncancerous cell lines L02 and C2C12. These noncancerous cell lines were each observed to be more sensitive to DOX compared to cancer cells.[58,59] Figure 8B shows that incubation of these cell lines with uncoated MSN^D particles resulted in significant loss in viability—again presumably due to leakage of DOX from these MSN^D particles. When cells were incubated with coated MSN^D particles, Figure 8B shows the DOX cytotoxicities were attenuated. Presumably, the intact multilayer inhibits nontargeted drug leakage. Further, Figure 8B shows the attenuated cytotoxicity of the coated MSN^D particles to L02 is unaffected by the addition of free transferrin to the incubation, again suggesting that those noncancerous cells lack enough transferrin receptor responsible for nanoparticle uptake. The same trend was also observed for the C2C12 cells, however, the reason could be explained by this mouse cells' lack of right receptor to human transferrin that we used for the coating assembly.

We performed one final study to demonstrate that the cytotoxicity of our coated MSN^D particles to HepG2 cells is consistent with the apoptotic mechanism reported for DOX-mediated cell killing.[60–63] Experimentally, we incubated HepG2 cells with $Tf/Con\ A(Gly/Con\ A)_4$–MSN^D (DOX dose 0.5 μg mL^{-1}) for 24 h after which the cells were fixed and examined. The fluorescence images in Figure 8C demonstrate uptake of the MSN^D particles (red fluorescence from Texas Red label) and intracellular release of the drug (green), while the fluorescence and bright field images show the cell shrinkage, chromatin condensation, and formation of apoptotic bodies characteristic of the apoptosis killing mechanism.

Overall, the results in Figure 8 demonstrate that the coated MSN^D particles have enhanced cytotoxicities for cancer cell lines but attenuated cytotoxicities for noncancerous cell lines (compared to uncoated MSN^D particles). These results also support the hypothesis that incorporation of transferrin into the coating confers targeting to cancer cells through upregulated transferrin receptors, binding to these receptors leads to

internalization through a receptor-mediated endocytosis mechanism, and the low endosomal pH triggers disassembly of the coating and release of the drug.

3. Conclusion

We report a self-assembling biologically based nanoparticle coating system that offers three important functional characteristics. First, the coating is based on sugar–lectin interactions that enable self-assembly of a multilayer of glycogen and Con A and the incorporation of the glycoprotein transferrin. Second, our results indicate that incorporation of transferrin into the coating confers selective targeting to cancer cell lines (cancer cells upregulate transferrin receptors) and induces cellular uptake (transferrin undergoes receptor mediated endocytosis). Finally, the Con A–glycogen coating disassembles at the low pHs that characterize endosomes, and this disassembly provides a mechanism for the triggered release of a nanoparticle cargo. In a proof-of-concept study, we applied this coating to the model of drug-loaded MSN and we observed enhanced cytotoxicities for cancer cell lines but attenuated cytotoxicities with noncancerous cells. More broadly, this work illustrates the potential for enlisting biology as a source of materials and mechanisms to perform advanced materials functions to meet the emerging demands for applications in the medical and life sciences (e.g., nanomedicine).

4. Experimental Section

Materials: Cetyltrimethylammonium bromide (CTAB) and tetraethylorthosilicate (TEOS) were purchased from Shanghai Lingfeng Chemical Reagent Co. Ltd., PEI, glycogen, D-glucose, and dithiodipropionic acid (DDPI) were purchased from TCI Development Co., Ltd. Con A, C FITC–Con A, and human transferrin were all purchased from Sigma Aldrich. (3-Aminopropyl) triethoxysilane (APTES) and Me-α-man were purchased from Aladdin. Texas Red was purchased from Santa Cruz. Doxorubicin was purchased from Shanghai Jingyan Chemical Science Co., Ltd. Gold-coated quartz crystal (QSX301Au) was purchased from Jiaxing Jingkong Electronics Co. Ltd. 4′,6-Diamidino-2-phenylindole (DAPI) and 3-(4,5-dimethylthiaol-2-yl)-2,5-diphenyltetrazolium bromide (MTT) were purchased from Beyotime Biotech Co. Ltd. All cell culture-related reagents were purchased from Gibco.

Preparation of MSN: The MSN particles are prepared according to the reported procedure.[27] Typically, CTAB serving as the template was first dissolved into the ammonia water. TEOS as the silica precursor was then added dropwise to the solution. The mixture was stirred for 2 h to give a white precipitate. The product was collected by centrifugation and washed with water and ethanol. The MSN particles were obtained after a high temperature calcination to remove the involved CTAB. To prepare the Texas Red-labeled MSN, we first modified the MSN with primary amines according to the reported procedure,[64] and then dispersed the particles into Na_2CO_3–$NaHCO_3$ buffer (pH 9.0). Texas Red solution in DMF was added dropwise into the particle suspension. After 8 h of stirring, the Texas Red-labeled MSN was collected by centrifugation, washed with buffer, and dried under vacuum.

Fabrication and Characterization of MSN with Coating: For the Con A–glycogen coating fabrication, the MSN particles (200 mg) were first incubated in PEI solution (4 mg mL^{-1}, 5 mL) for 30 min to modify the particle surface with positive charges. The particles were then sequentially contacted with solutions containing Con A and glycogen alternatively each for 30 min (2 mg mL^{-1}, in Tris-HCl containing 1×10^{-1} M Mn^{2+} and 1×10^{-1} M Ca^{2+} buffered at pH 7.8, 5 mL). After each assembly, the particles were centrifuged (8000 rpm, 10 min) and washed twice with Tris-HCl buffer. The Con A–glycogen coating was obtained after several repeated adsorption steps, and denoted as Con A(Gly/Con A)$_n$–MSN or (Gly/Con A)$_n$–MSN, there n represents the recycle number. For the fluorescence study, FITC-labeled Con A was employed instead of Con A to fabricate the coating. For the Con A–glycogen–transferrin coating fabrication, Con A(Gly/Con A)$_4$–MSN was first incubated with a solution containing transferrin (4 mg mL^{-1}, in Tris-HCl containing 1×10^{-1} M Mn^{2+} and 1×10^{-1} M Ca^{2+} buffered at pH 7.8, 5 mL) for 30 min, and then removed from the liquid by centrifugation. The free transferrin left in the supernatant was quantified by UV–vis at 465 nm. The amount of transferrin associated with the NPs was calculated by subtracting the free molecules from the total feeding amount and give the binding ratio of 80 μg (Tf) mg^{-1} (coated-MSN). The morphology of the coating was examined by a JEM-2100 transmission electron microscopy (TEM) (JEOL, Japan). TGA of the coating content was performed using a STA 409-PC thermal analyzer (Netzsch, Germany). FTIR analysis was performed using a Nicolet 5700 FTIR spectrophotometer (ThermoElectron, USA).

Drug Loading: (Gly/Con A)$_4$–MSN or Tf/Con A(Gly/Con A)$_4$–MSN particles were dispersed in DOX solution (4 mg mL^{-1}, 5 mL, pH 7.4) and stirred for 12 h, followed by centrifugation and washing steps to remove any free DOX from the outside of the particles. The sample was freeze-dried and denoted as (Gly/Con A)$_4$–MSN^D or Tf/Con A(Gly/Con A)$_4$–MSN^D, respectively. Nitrogen adsorption–desorption measurement was performed on an adsorption analyser ASAP2010N (Micrometrics, Inc., USA). The surface areas and pore volumes were calculated by the Brunauer–Emmett–Teller (BET) method. Pore size was estimated by the Barrett–Joyner–Halenda (BJH) method.

Quantitative Study of Coating Disassembly and Drug Release: For the pH-response studies, 10 mg of (Gly/Con A)$_4$–MSN (FITC–Con A) or drug-loaded (Gly/Con A)$_4$–MSN^D particles were suspended in 1 mL of buffer solutions with varying pHs (4.0, 5.0, 5.5, 6.0, 6.8, and 7.4). At each time interval, the supernatant was taken out by centrifugation for measurement, and an equal volume of fresh buffer was added instead. The fluorescence measurement for the coating disassembly was performed using SpectraMax (M2, USA) at λ_{ex} = 488 nm and λ_{em} = 525 nm, and the UV–vis measurement for the drug release was performed at the wavelength of 485 nm using the same instrument. For the glucose stability studies, the experimental conditions were the same except the buffer solutions were added with glucose (5×10^{-3}, 25×10^{-3}, and 125×10^{-3} M).

Sugar–Lectin Interaction Analysis by ITC: ITC was employed to study the interactions between Con A and glycol–ligands (glucose, Me-α-man, and transferrin). The experiments were performed using microcalorimeter Microcal ITC 200. Tris-HCl buffer (10×10^{-3} M, pH 7.8) containing NaCl (0.9 M), $CaCl_2$ (1×10^{-3} M), and $MnCl_2$ (1×10^{-3} M) was filtered, thoroughly degassed, and used for preparing the Con A and glycol–ligand solutions. In each titration, 1.5 μL of ligand solution (glucose, Me-α-man, and Tf) was injected into the Con A solution with a time interval of 2 min at 25 °C. The heat evolved during the binding process was measured. The data were fitted to a one-site binding model using a nonlinear least-squares procedure and give the binding affinity K_a and enthalpy ΔH.

Coating (Multilayer) Assembly/Disassembly Monitored by QCM-D: The assembly and response process of the multilayer were monitored by QCM-D (Q-Sense E1, Sweden) using gold-coated quartz crystals (5 MHz) as substrates. For the multilayer growth monitoring, the crystal was first modified with PEI, followed by alternate assembly of Con A and glycogen layers. Buffer rinsing was performed for 5–10 min after each assembly. For the pH or glucose-response investigation, the multilayer was assembled offline on the crystals and then subjected to acidic buffer or glucose solutions. Buffer rinsing was also performed after each treatment. The crystals frequency shifts at varying overtones were monitored during the whole process.

Cell Lines: The human hepatoma cell line HepG2, human breast adenocarcinoma cell line MDA-MB-231, human gastric cancer cell line MGC-803, human hepatic cell line L02, mouse myoblast cell line C2C12

were all purchased from the American Type Culture Collection (ATCC). Cell cultures were performed in Dulbecco's modified Eagle's medium (DMEM; GIBCO) supplemented with 10% fetal bovine serum (FBS), 1% penicillin, and 1% streptomycin.

Targeting Effect Assay by Flow Cytometry: The cells were seeded at a concentration of 2×10^5 cells/well. After the incubation for 24 h, the cell media were removed from the wells and fresh media supplemented with Texas Red-labeled MSN, Con A(Gly/Con A)$_4$–MSN, and Tf/Con A(Gly/Con A)$_4$–MSN at 50 μg mL^{-1} were added. After another 3 h incubation, the media were removed, and the cells were washed with PBS and harvested by trypsinization. To quench extracellular fluorescence, the cells were treated with trypan blue for 10 min. The cells were then washed and dispersed into PBS. The amount of endocytosed particles inside cells were analyzed by fluorescence-activated cell sorting (FACS) in a Becton–Dickinson FACS Canto flow cytometry.

Fluorescence Confocal Imaging: The cells were seeded at a density of 2×10^4 cells/well and incubated for 24 h. For intracellular coating disassembly study, the cell media were replaced by fresh media supplemented with Tf/Con A(Gly/Con A)$_4$–MSN (Texas Red-labeled MSN and FITC-labeled Con A) at a concentration of 20 μg mL^{-1}. For intracellular drug release study, the media were replaced by suspensions of MSN^D or Tf/Con A(Gly/Con A)$_4$–MSN^D (Texas Red-labeled MSN) at a Dox level of 0.5 μg mL^{-1}. For targeting effect study, the media were replaced by suspensions of MSN, Con A(Gly/Con A)$_4$–MSN, or Tf/Con A(Gly/Con A)$_4$–MSN (Texas Red-labeled MSN) at a concentration of 50 μg mL^{-1}. For free transferrin competition study, the cells were pretreated with transferrin (200 μg mL^{-1}) for 0.5 h prior to the addition of the particles. After a certain period of incubation, the media were removed and the cells were washed with PBS. The cells were fixed with glutaraldehyde and stained with DAPI for 15 min. The fluorescence images were taken by Nikon A1R confocal microscope at λ_{ex} = 404 nm and λ_{em} = 450 nm for DAPI, λ_{ex} = 488 nm and λ_{em} = 525 nm for Dox/FITC–Con A, and λ_{ex} = 561 nm and λ_{em} = 595 nm for Texas Red observations. In order to semiquantify the disassembly and the DOX release, photomultiplier gain were kept constant for a certain set of experiment.

Cytotoxicity Assay by MTT: The cells were seeded at a density of 2×10^4 cells/well and incubated for 24 h. After that the cell media were replaced by fresh media supplemented with MSN^D, Tf/Con A(Gly/Con A)$_4$–MSN^D, or Tf/Con A(Gly/Con A)$_4$–MSN^D. The DOX level was 2 μg mL^{-1}. After 48 h of culture, the media were removed and the cells were washed with PBS. 1 mL of culture media containing 1 mg mL^{-1} MTT were added to each well and the plates were incubated for another 4 h. The yielded purple formazan crystals inside cells were dissolved by DMSO and OD values were measured at 492 nm using a Spectramax M2 plate reader (Molecular Devices, USA). For free transferrin competition study, the cells were pretreated with transferrin (200 μg mL^{-1}) for 0.5 h prior to the addition of the particles. For the biocompatibility assay of the coating, the MSN or Tf/Con A(Gly/Con A)$_4$–MSN were, respectively, incubated with cells for 24/48 h at varying concentrations. The cell viability was examined by the same MTT method.

Cell Apoptosis Assay by Confocal Microscope: The cells were cultured with Tf/Con A(Gly/Con A)$_4$–MSN^D (Texas Red MSN) under the same procedure as described in *Fluorescence Confocal Imaging* part with DOX level of 0.5 μg mL^{-1}. After 24 h incubation, the cells were stained with DAPI and examined by confocal microscope.

Supporting Information

Supporting Information is available from the Wiley Online Library or from the author.

Acknowledgements

The authors acknowledge the financial support from the National Basic Research Program of China (2012CB933600), the National Natural Science Foundation of China (51103043), the 111 project (B14018), Shanghai Natural Science Foundation (11ZR1409100), Innovation Program of Shanghai Municipal Education Commission (14ZZ060), the Fundamental Research Funds for the Central Universities (WD1214056), Shanghai Science and Technology Development Funds (14QA1401000), and the Robert W. Deutsch Foundation.

Received: October 17, 2014
Published online: January 21, 2015

[1] O. Shimoni, A. Postma, Y. Yan, A. M. Scott, J. K. Heath, E. C. Nice, A. N. Zelikin, F. Caruso, *ACS Nano* **2012**, *6*, 1463.
[2] A. Johnston, M. Kamphuis, G. Such, *ACS Nano* **2012**, *6*, 6667.
[3] D. P. Ferris, J. Lu, C. Gothard, R. Yanes, C. R. Thomas, J. C. Olsen, J. F. Stoddart, F. Tamanoi, J. I. Zink, *Small* **2011**, *7*, 1816.
[4] C. C. E. Ashley, E. C. E. Carnes, G. K. G. Phillips, D. Padilla, P. N. Durfee, P. A. Brown, T. N. Hanna, J. Liu, B. Phillips, M. B. Carter, *Nat. Mater.* **2011**, *10*, 389.
[5] P. Zhang, F. Cheng, R. Zhou, J. Cao, J. Li, C. Burda, Q. Min, J.-J. Zhu, *Angew. Chem. Int. Ed.* **2014**, *53*, 2371.
[6] G. F. Payne, E. Kim, Y. Cheng, H.-C. Wu, R. Ghodssi, G. W. Rubloff, S. R. Raghavan, J. N. Culver, W. E. Bentley, *Soft Matter* **2013**, *9*, 6019.
[7] A. Schlossbauer, S. Warncke, P. M. E. Gramlich, J. Kecht, A. Manetto, T. Carell, T. Bein, *Angew. Chem. Int. Ed.* **2010**, *49*, 4734.
[8] A. Schlossbauer, J. Kecht, T. Bein, *Angew. Chem.* **2009**, *121*, 3138.
[9] K. Sato, D. Kodama, J. Anzai, *Anal. Bioanal. Chem.* **2006**, *386*, 1899.
[10] K. Sato, Y. Imoto, J. Sugama, S. Seki, H. Inoue, T. Odagiri, T. Hoshi, J. Anzai, *Langmuir* **2005**, *21*, 797.
[11] K. Sato, D. Kodama, Y. Endo, J.-I. Anzai, *J. Nanosci. Nanotechnol.* **2009**, *9*, 386.
[12] Y. Zhu, W. Tong, C. Gao, *Soft Matter* **2011**, *7*, 5805.
[13] Y. Lvov, K. Ariga, I. Ichinose, T. Kunitake, *Thin Solid Films* **1996**, *284*, 797.
[14] Y. Lvov, K. Ariga, I. Ichinose, T. Kunitake, *J. Chem. Soc., Chem. Commun.* **1995**, *117*, 2313.
[15] H. Yang, Q. An, W. Zhu, W. Li, Y. Jiang, J. Cui, X. Zhang, G. Li, *Chem. Commun.* **2012**, *48*, 10633.
[16] K. Liu, Y. Kang, Z. Wang, X. Zhang, *Adv. Mater.* **2013**, *25*, 5530.
[17] H. Yang, B. Yuan, X. Zhang, O. A. Scherman, *Acc. Chem. Res.* **2014**, *47*, 2106.
[18] T. R. Daniels, T. Delgado, G. Helguera, M. L. Penichet, *Clin. Immunol.* **2006**, *121*, 159.
[19] L.-Z. Luo, H.-W. Jin, H.-Q. Huang, *J. Proteom.* **2012**, *77*, 237.
[20] T. R. Daniels, E. Bernabeu, J. A. Rodríguez, S. Patel, M. Kozman, D. A. Chiappetta, E. Holler, J. Y. Ljubimova, G. Helguera, M. L. Penichet, *Biochim. Biophys. Acta* **2012**, *1820*, 291.
[21] K. M. Mayle, A. M. Le, D. T. Kamei, *Biochim. Biophys. Acta* **2012**, *1820*, 264.
[22] X. Zeng, Y.-X. Sun, W. Qu, X.-Z. Zhang, R.-X. Zhuo, *Biomaterials* **2010**, *31*, 4771.
[23] R. F. Murphy, *J. Cell Biol.* **1984**, *98*, 1757.
[24] T. K. Dam, S. Oscarson, R. Roy, S. K. Das, D. Pagé, F. Macaluso, C. F. Brewer, *J. Biol. Chem.* **2005**, *280*, 8640.
[25] W. Tong, Y. Zhu, C. Gao, *Colloid Polym. Sci.* **2011**, *290*, 233.
[26] S. Chinnayelka, M. J. McShane, *J. Fluoresc.* **2004**, *14*, 585.
[27] F. Caruso, E. Rodda, D. N. Furlong, K. Niikura, Y. Okahata, *Anal. Chem.* **1997**, *69*, 2043.
[28] F. Caruso, D. Furlong, K. Niikura, Y. Okahata, *Colloids Surf. B* **1998**, *10*, 199.
[29] F. Boulmedais, V. Ball, P. Schwinte, B. Frisch, *Langmuir* **2003**, *19*, 440.
[30] Q. Gan, X. Lu, Y. Yuan, J. Qian, H. Zhou, X. Lu, J. Shi, C. Liu, *Biomaterials* **2011**, *32*, 1932.

[31] H. E. Auer, T. Schilz, *Int. J. Pept. Protein Res.* **1984**, *24*, 462.
[32] D. F. Senear, D. C. Teller, *Biochemistry* **1981**, *20*, 3076.
[33] J. Zhang, Z. F. Yuan, Y. Wang, W. H. Chen, G. F. Luo, S. X. Cheng, R. X. Zhuo, X. Z. Zhang, *J. Am. Chem. Soc.* **2013**, *135*, 5068.
[34] Q. Zhang, F. Liu, K. T. Nguyen, X. Ma, X. Wang, B. Xing, Y. Zhao, *Adv. Funct. Mater.* **2012**, *22*, 5144.
[35] A. Bernardos, L. Mondragon, E. Aznar, M. D. Marcos, R. Martinez-Mañez, F. Sancenon, J. Soto, J. M. Barat, E. Perez-Paya, C. Guillem, P. Amoros, *ACS Nano* **2010**, *4*, 6353.
[36] G. H. McKenzie, W. H. Sawyer, L. W. Nichol, *Biochim. Biophys. Acta* **1972**, *263*, 283.
[37] J. B. Corbell, J. J. Lundquist, E. J. Toone, *Tetrahedron: Asymmetry* **2000**, *11*, 95.
[38] Y. Shiraishi, M. Akiyama, T. Sato, M. Hattori, T. Komatsu, *Polym. Adv. Technol.* **2014**, *25*, 1247.
[39] D. Mann, M. Kanai, *J. Am. Chem. Soc.* **1998**, *120*, 10575.
[40] R. Kornfeld, C. Ferris, *J. Biol. Chem.* **1975**, *250*, 2614.
[41] Y. Gou, S. Slavin, J. Geng, L. Voorhaar, D. M. Haddleton, C. R. Becer, *ACS Macro Lett.* **2012**, *1*, 180.
[42] D. Formanowicz, P. Formanowicz, *Int. Urol. Nephrol.* **2012**, *44*, 907.
[43] D. Steverding, D. W. Sexton, N. Chrysochoidi, F. Cao, *Mol. Biochem. Parasitol.* **2012**, *185*, 99.
[44] O. Choi, N. Tomiya, J. H. Kim, J. M. Slavicek, M. J. Betenbaugh, Y. C. Lee, *Glycobiology* **2003**, *13*, 539.
[45] K. J. Brown, A. Vanderver, E. P. Hoffman, R. Schiffmann, Y. Hathout, *Int. J. Mass Spectrom.* **2012**, *312*, 97.
[46] D. K. Mandal, N. Kishore, C. F. Brewer, *Biochemistry* **1994**, *33*, 1149.
[47] B. N. Murthy, S. Sinha, A. Surolia, N. Jayaraman, L. Szilagyi, I. Szabo, K. E. Kover, *Carbohydr. Res.* **2009**, *344*, 1758.
[48] B. W. Sigurskjold, *Anal. Biochem.* **2000**, *277*, 260.
[49] A. Salvati, A. S. Pitek, M. P. Monopoli, K. Prapainop, F. B. Bombelli, D. R. Hristov, P. M. Kelly, C. Åberg, E. Mahon, K. A. Dawson, *Nat. Nanotechnol.* **2013**, *8*, 137.
[50] J. Wang, S. Tian, R. A. Petros, M. E. Napier, J. M. Desimone, *J. Am. Chem. Soc.* **2010**, *132*, 11306.
[51] W. Fang, Z. Wang, S. Zong, H. Chen, D. Zhu, Y. Zhong, Y. Cui, *Biosens. Bioelectron.* **2014**, *57*, 10.
[52] C. Tekle, B. Van Deurs, K. Sandvig, T.-G. Iversen, *Nano Lett.* **2008**, *8*, 1858.
[53] B. D. Chithrani, W. C. W. Chan, *Nano Lett.* **2007**, *7*, 1542.
[54] Z. M. Qian, H. Li, H. Sun, K. Ho, *Pharmacol. Rev.* **2002**, *54*, 561.
[55] A. Ciechanover, A. L Schwartz, H. F. Lodish, *Cell* **1983**, *32*, 267.
[56] T. Tanaka, Y. Fujishima, Y. Kaneo, *Biol. Pharm. Bull.* **2001**, *24*, 268.
[57] S. Aroui, S. Brahim, M. De Waard, A. Kenani, *Biochem. Biophys. Res. Commun.* **2010**, *391*, 419.
[58] X. Cheng, F. Zhang, G. Zhou, S. Gao, L. Dong, W. Jiang, Z. Ding, J. Chen, J. Zhang, *Drug Delivery* **2009**, *16*, 135.
[59] H. Chen, Z. Luo, W. Sun, C. Zhang, H. Sun, N. Zhao, J. Ding, M. Wu, Z. Li, H. Wang, *Cancer Lett.* **2013**, *336*, 204.
[60] T. Lee, T. Lau, I. Ng, *Cancer Chemother. Pharmacol.* **2002**, *49*, 78.
[61] A.-M. M. Osman, H. M. Bayoumi, S. E. Al-Harthi, Z. A. Damanhouri, M. F. Elshal, *Cancer Cell Int.* **2012**, *12*, 47.
[62] Q. Zhang, X. Wang, P.-Z. Li, K. T. Nguyen, X.-J. Wang, Z. Luo, H. Zhang, N. S. Tan, Y. Zhao, *Adv. Funct. Mater.* **2014**, *24*, 2450.
[63] H. Meng, M. Liong, T. Xia, Z. Li, Z. Ji, J. I. Zink, A. E. Nel, *ACS Nano* **2010**, *4*, 4539.
[64] X. Huang, X. Teng, D. Chen, F. Tang, J. He, *Biomaterials* **2010**, *31*, 438.